Non-LTE Modeling of the Structure and Spectra of Hot Accretion Spots on the Surface of Young Stars

A. V. Dodin*

Sternberg Astronomical Institute, Moscow State University, Universitetskii pr. 13, Moscow, 119992 Russia Received November 17, 2014

Abstract—The results of modeling the structure and spectra of hot accretion spots on the surface of young stars with allowance made for the departures from LTE for hydrogen and helium are presented. The existence of ram pressure of the infalling gas at the outer boundary of the hot spot has been found to lead to Stark broadening of the hydrogen line profiles to $\sim 1000 \text{ km s}^{-1}$ at the accretion parameters considered. It is shown that allowance for the departures from LTE for carbon and oxygen atoms and ions does not lead to noticeable changes in the structure of the hot spot.

DOI: 10.1134/S1063773715050023

Keywords: stars—individual: TW Hya, T Tauri stars, stellar atmospheres, radiative transfer, spectra.

INTRODUCTION

Classical T Tauri stars (CTTS) are young (ages $<10^7$ yr) stars with masses $<3~M_{\odot}$ at the stage of gravitational contraction to the main sequence whose activity is attributable to the magnetospheric accretion of matter from a protoplanetary disk. The optical spectrum of CTTS consists of the absorption spectrum of a late-type star on which emission lines with nontrivial profiles of variable shape are superimposed. Generally speaking, the emission lines consist of two components: narrow (FWHM $\sim 30 \text{ km s}^{-1}$) and broad (FWHM > 100 km s⁻¹) ones that are formed in different spatial regions (see, e.g., Batalha et al. 1996; Dodin et al. 2012). The flux ratio of these components is different for different lines and changes with time, while for identical lines it changes from star to star.

There is little doubt that the theory of magnetospheric accretion, in principle, is capable of explaining the profiles, relative intensity, and complex variability of emission lines in the spectra of CTTS if the nontrivial kinematics of the gas and the variety of physical conditions in the immediate vicinity of the star predicted by this theory are taken into account (Königl 1991; Romanova et al. 2004). Within the framework of the magnetospheric model, the accreting disk gas at some distance from the star is frozen into the stellar magnetic field. In doing so, the gas must first reduce its angular velocity to that of the

stellar magnetic field, which must be accompanied by gas heating at the magnetospheric boundary and by its partial outflow into the surrounding space. Since the typical linear velocities at the magnetospheric boundary are hundreds of km s $^{-1}$, this region is well suited for the formation of broad emission line components (Gomez de Castro and Rekowski 2011).

The gas frozen in the magnetic field flows down toward the star under the force of attraction, and this infalling gas can also manifest itself in the spectrum as broad line components (see, e.g., Petrov et al. 2014), which can be redshifted by a value that does not exceed the free-fall velocity near the stellar surface:

$$V_0 = \sqrt{\frac{2GM_*}{R_*}} \left(1 - \frac{R_*}{R_0} \right)^{1/2},$$

where M_* and R_* are the stellar mass and radius, R_0 is the distance from which the gas begins to fall freely along the magnetic field lines.

Having reached the dense layers of the stellar atmosphere, the matter decelerates in the accretion shock, converting the bulk of its kinetic energy into heat, with its flux being

$$F_{\rm acc} = \frac{\mu m_p N_0 V_0^3}{2},$$

where N_0 and V_0 are the pre-shock gas number density and velocity, $\mu \approx 1.26$ is the mean molecular weight of the atomic nucleus for solar elemental abundances, and m_p is the proton mass. The hot post-shock matter cools down, losing its energy

^{*}E-mail: dodin_nv@mail.ru

through UV and X-ray radiation, and settles to the stellar surface, gradually reducing its velocity almost to zero. This accretion shock radiation and the radiation of the infalling gas irradiate the underlying stellar atmosphere, producing a hot spot on the stellar surface, which manifests itself in the spectra as narrow emission line components and which causes a reduction in the depths of absorption lines in the spectra of CTTS compared to the spectra of main-sequence stars of the same spectral type.

Calvet and Gullbring (1998) calculated the hotspot radiation in continuum, while Dodin and Lamzin (2012) took into account numerous spectral lines in their LTE calculations of the hot-spot structure and spectrum. In their subsequent paper, Dodin et al. (2013) showed the He II lines to exhibit large departures from LTE and to be informative for diagnosing the shock parameters. Large departures from LTE in He I and He II, which are the main absorbers of the incident radiation, can change the distribution of parameters in the atmosphere. However, Dodin et al. (2013) took the distribution of parameters and the radiation field from an LTE model, which, as a result, did not allow the HeI lines to be used for diagnostics and gave impetus to the construction of a non-LTE model atmosphere.

The modeling of the hot-spot structure and spectrum considered in this paper and in Dodin and Lamzin (2012) is among the problems of atmospheric heating by external radiation that have been repeatedly solved by various authors (see, e.g., Mitskevich and Tsymbal 1992; Sakhibullin and Shimanskii 1996; Günther and Wawrzyn 2011). However, when applied to CTTS, this problem has a number of peculiarities that eventually change the results qualitatively. The main peculiarity is the existence of ram pressure of the infalling gas at the outer boundary of the atmosphere, which must lead to an increase in density in the irradiated atmosphere and to a decrease in the departures from LTE compared to the case where there is no external pressure. Furthermore, in our problem the source of ionizing radiation is immediately adjacent to the atmosphere being heated, irradiating it simultaneously on all sides, in contrast to binary systems where the source of external radiation is at a considerable distance from the star, and, consequently, the radiation enters the atmosphere from a considerably smaller solid angle.

THE METHODS OF CALCULATIONS

In this paper, we will arbitrarily divide the accretion zone in the vertical direction into three parts: the preshock region, the post-shock region of settling gas, and the hot spot. Whereas there exists a physical boundary in the form of an accretion shock front

between the pre-shock region of freely falling gas and the post-shock region, no strict boundary can be drawn between the post-shock region of gas settling and the hot spot. Therefore, here by the post-shock region of gas settling we mean the post-shock region calculated by Lamzin (1998). The gas in this region is transparent in continuum and gradually radiates almost all of the energy released in the accretion shock, virtually reaching statistical and radiative equilibrium at the lower boundary of the region, which simultaneously is the upper boundary of the hot spot. The optical depths considered here are measured from this boundary, and, therefore, they cover neither the postshock region of gas settling nor the pre-shock region. These regions are considered as outer envelopes and are taken into account separately. Simultaneously modeling all regions still remains an excessively complex computational problem, and, at this juncture, the mutual influence of the pre-shock region of freely falling gas and the hot spot is taken into account by successive approximations in two steps: first the structure and spectrum of the pre-shock region are calculated using a primitive hot-spot model, and then the radiation obtained is used to model the hot spot itself (see the Appendix in Dodin and Lamzin 2012). Performing yet another iteration leads to a change in the integrated flux approximately by 5% in the worst case, and, therefore, it was not performed in view of the remaining uncertainties of such a scale.

Within the framework of such a division of the accretion zone, the hot accretion spot will be considered as a plane-parallel stellar atmosphere in hydrostatic and radiative equilibrium. Thus, we ignore the residual gas motion and the advection of energy both from the post-shock cooling region into the hot spot and within the hot spot. To compute the model of such an atmosphere, a numerical self-consistent solution of the system of equations described below is performed.

- (1) The *hydrostatic equilibrium equation*, which is solved by taking into account the external pressure from the infalling gas. The equation includes only the gas and radiation pressures. The pressure from the magnetic field or turbulence is disregarded.
- (2) The Saha and Boltzmann equations for all atoms and ions of the elements from H to Zn.
- (3) The statistical equilibrium equations for atoms and ions treated in non-LTE. The equations are solved only for a few selected elements; the corresponding atomic data are given in the next section.
- (4) The *radiative transfer equation*, which is solved by taking into account the incident radiation at the upper boundary.

To construct a model that adequately describes real stellar atmospheres, the gas opacity should be

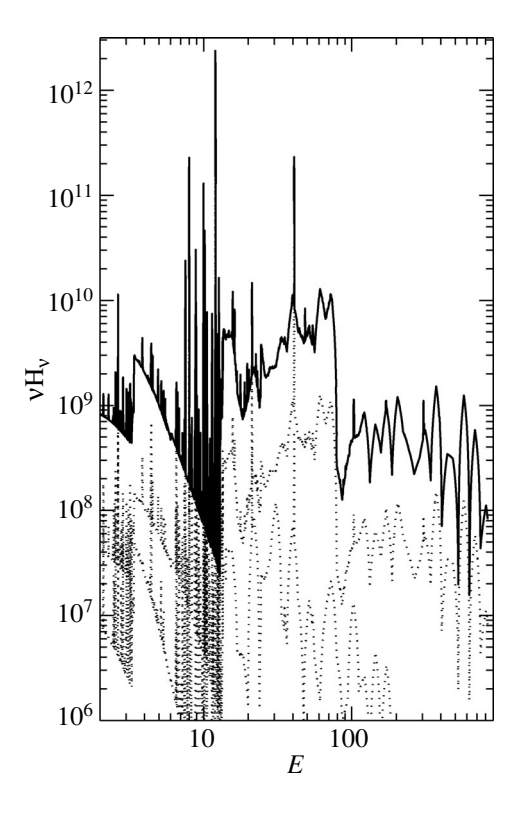


Fig. 1. External radiation spectrum for various accretion parameters: $V_0 = 200 \text{ km s}^{-1}$, $\log N_0 = 11.5 \text{ (dotted line)}$; $V_0 = 400 \text{ km s}^{-1}$, $\log N_0 = 11.5 \text{ (dash-dotted line)}$; $V_0 = 400 \text{ km s}^{-1}$, $\log N_0 = 12.5 \text{ (solid line)}$. The product of frequency and Eddington flux [erg s⁻¹ cm⁻² sr⁻¹] is shown as a function of photon energy E [eV].

properly calculated. In our models, when solving the radiative transfer equation, we take into account the line and continuum opacity (f—b and f—f) for elements treated in LTE and non-LTE, the opacity related to H^- , the Rayleigh and Thomson scattering. Since the molecular opacity is disregarded, the code cannot be applied to model the atmospheres of cool stars; however, there must be no molecules in the hot spot we consider. For LTE elements, when computing the model atmospheres, we take into account the opacity in numerous lines by the opacity sampling method for more than 60 000 frequency points. In the final calculation of the spectrum, the number of frequency points in the range 3000-12000 Å of interest to us was increased to 180000, which allows the profiles of individual lines to be roughly calculated. The line opacity for non-LTE elements is taken into account directly: the profiles of all lines are accurately calculated on special frequency grids for each line.

The external radiation acting as a boundary condition in the radiative transfer equation is calculated in a similar way as was done in Dodin and Lamzin (2012), with the only exception that the most convenient

frequency grid can now be used. This grid is a combination of the frequency grids on which the various components of the external radiation were calculated. There are two such components. The first component is the shock radiation that was calculated by Lamzin (1998) in the form of a set of pseudo-lines and signal lines. Since only the fluxes are given for the signal lines in this paper, for definiteness the shape of a Doppler profile with a width and redshift of $V_0/8$ was imparted to the lines. Testing showed that the result does not depend on the chosen parameters of these profiles. The second component of the external radiation is the radiation from the pre-shock gas, which was calculated with the Cloudy code (Ferland et al. 1998) in exactly the same way as was done in Dodin and Lamzin (2012). A few examples of the external radiation spectrum are shown in Fig. 1. Neither the data from Lamzin (1998) nor the Cloudy code allows the angular intensity distribution of the incident radiation to be determined. Therefore, just as in Dodin and Lamzin (2012), we will assume it to be isotropic.

(5) The equations of radiative equilibrium and constancy of total (radiative and convective) energy flux in depth. The energy flux transferred by convection is calculated within the framework of the mixing-length theory with $\alpha = 1.25$.

The balance between gas heating and cooling and a constant energy flux through the atmosphere in the case of only radiative transfer are achieved by the temperature correction method from Dreizler (2003). The modified Avrett—Krook scheme from the ATLAS9 code (Kurucz 1970; Castelli and Kurucz 2004) is used in the convection zone.

The DETAIL code (Butler and Giddings 1985), which allows equations 2-4 to be solved self-consistently by the accelerated Λ -iteration method, forms the basis for the computer code that solves these equations. At the first iteration, these equations are solved for an initial model taken from the LTE calculations described by Dodin and Lamzin (2012). Then, this model is corrected to satisfy conditions 1 and 5. The corrected model is used to solve again equations 2-4 and to calculate new corrections to the model. The iterations are repeated until all equations are satisfied with the desired accuracy. A more detailed description of the code, its testing, and comparison with the results of other codes for various model atmospheres can be found on the web page. ¹

ATOMIC DATA

Non-LTE calculations require critically selected atomic data whose volume increases considerably

lnfm1.sai.msu.ru/~davnv/hotspot

compared to LTE calculations. In selecting the atomic data for hydrogen and helium, we will adhere to the recommendations from Przybilla and Butler (2004) and Przybilla (2005). Comparison of our atomic data with other data and their testing can be found on the web page.² The model atmosphere and the emergent radiation were calculated with the same set of atomic data. All of the atomic data needed to calculate the LTE models are equal to the corresponding data used in our non-LTE modeling. All spectral lines of all elements were calculated by assuming a complete frequency redistribution.

Hydrogen Model Atom

Our testing showed that the model atom that includes all levels up to n=20 is enough to calculate the structure and spectra of various stellar atmospheres and, in particular, to calculate the hotspot spectrum. The level energies were calculated using the Rydberg formula by taking into account the reduction of the ionization potential by the energy of the 21st level at which the continuum is assumed to start:

$$E_H = R_H \left(\frac{1}{n^2} - \frac{1}{21^2}\right).$$

Our testing on model stellar atmospheres without external radiation showed the appropriateness of such a procedure. However, in the problem under consideration, the models and spectra calculated with and without the reduction of the ionization potentials barely differ from one another (by less than 1% in the $H\alpha-H\delta$ lines). The line wavelengths are determined from the level energies except the Balmer series, where the VALD data (Kupka et al. 1999) are used.

The oscillator strengths of the transitions were calculated using formulas from Berestetskii et al. (1982). The profiles of the lines corresponding to the transitions from n=1-4 to all higher-lying levels were calculated by taking into account the Stark broadening: the tables of Stehle and Hutcheon (1999) were used for the lines of all transitions from n=1-3 to $n \le 7$; for the remaining lines with a lower level n=1-4, the profile was calculated using the theory of Griem (1960) in the realization of Auer and Mihalas (1972). The remaining lines have Doppler profiles.

Allowance for a sufficiently large number of levels in the model atom and the Stark broadening for the transitions even from highly excited levels is needed to correctly describe the spectra near the ionization thresholds. A simplified consideration of the lines

near the series limit will lead to an error in the integrated flux and, consequently, to an error in the model atmosphere.

The electron-impact excitation and deexcitation rates are calculated just as in Przybilla and Butler (2004) and correspond to model E from this paper.

The electron-impact ionization rate is calculated according to Johnson (1972).

The photoionization cross sections for H I are calculated using the formula for hydrogenic ions with the Gaunt factor g_{II} from Przybilla and Butler (2004).

He I Model Atom

The helium model atom includes all levels up to the principal quantum number n=10. The level energies were taken from the NIST database and were reduced by the energy of the 11th level just as was done for hydrogen. As in Przybilla (2005), the individual levels differing by L and S are considered up to n=5, while all of the higher levels for each n are combined in L into singlet and triplet spin systems. Our testing showed that a detailed consideration of the atomic levels up to n=7 did not lead to a significant change of the results in the lines of interest to us.

The line wavelengths and oscillator strengths were taken from the NIST database and were supplemented by data from the NORAD database³ (Nahar 2010). The Stark broadening was taken into account using the tables from Dimitrijevic and Sahal-Brechot (1984). The lines for which there are no data on their Stark broadening were specified by Doppler profiles. Many helium lines have a multicomponent structure that leads to a significant broadening and distortion of the profiles. Therefore, the profile $\varphi(\lambda)$ for such lines is calculated as the profile of all fine-structure components averaged over gf:

$$\varphi(\lambda) = \frac{\sum g_i f_i \phi(\lambda - \lambda_i)}{\sum g_i f_i}.$$

The electron-impact excitation (and deexcitation) rates for all transitions from n=1,2 (except the $2p^1P$ level) to n=2-5 were taken from the tables in Bray et al. (2000). We calculated the remaining allowed transitions according to Mihalas and Stone (1968) and the forbidden transitions using a formula from Allen (1973).

The electron-impact ionization rates for He I are calculated using formulas from Mihalas and Stone (1968).

The photoionization cross sections for all levels with $n \le 7$ were taken from the NORAD database (Nahar 2010). The photoionization cross sections for the levels with n = 8-10 were calculated using the formula for a hydrogenic atom.

²lnfm1.sai.msu.ru/~davnv/hotspot

³ http://www.astronomy.ohio-state.edu/~nahar/

He II Model Atom

The ionized helium model atom includes 40 levels. The ionization energy from each level and the oscillator strengths of the transitions were calculated in the same way as for hydrogen.

The profiles of the lines corresponding to the transitions from n=1-4 to higher-laying levels were calculated by taking into account the Stark broadening. The 4686 and 1640 Å line profiles were calculated using the tables from Schöning and Butler (1989) with allowance made for the multicomponent structure of the lines. The remaining lines have Doppler profiles.

The electron-impact excitation and deexcitation rates for the transitions from n=1-2 to n=2-5 were taken from the CHIANTIv.5.0 database (Dere et al. 1997; Landi et al. 2006). The theory of Percival and Richards (1978) was used for the transitions between levels with $n \geq 5$. A formula from Mihalas (1972) was used for the remaining transitions.

The electron-impact ionization rates for He II for the first seven levels were calculated according to Clark et al. (1991). An approximate formula from Seaton (1962) was used for the remaining levels.

The photoionization cross sections for He II were calculated similarly to those for hydrogen.

C I—IV and O I—IV Model Atoms

To qualitatively estimate the influence of non-LTE effects in carbon and oxygen on the model atmosphere, we used simplified C I—IV and O I—IV model atoms. The energy levels chosen for our calculations are given in Tables 1 and 2. Close excited energy levels are combined into a single level when their populations are calculated, but the structure of these combined levels is taken into account in the same way as was done for the fine structure of helium lines when the spectrum is calculated. Such a procedure allows a large number of spectral lines to be taken into account, while the number of atomic levels is small.

The level energies and statistical weights were taken from NIST. The line wavelengths, oscillator strengths, and damping constants (if available) were taken from VALD (Kupka et al. 1999) and were supplemented by data from NIST and, in the case of C II, from Fischer and Tachiev (2004). The electronimpact excitation and deexcitation rates were taken from Reid (1994) for C I, from Wilson et al. (2005) for C II, from Mitnik et al. (2003) for C III, from Griffin et al. (2000) for C IV, from Barclem (2007) and Bhatia and Kastner (1995) for O I, from Kisielius et al. (2009) and McLaughlin and Bell (1994) for O II, from Aggarwal and Keenan (2008) for O IV. The rates missing

in the literature were calculated using the van Regemorter (1962) formula for allowed transitions and the Allen (1973) formula for forbidden transitions. The photoionization cross sections for all atoms and ions were taken from the NORAD database (see Nahar and Pradhan 1991, 1994, 1997; Nahar 1994, 1995, 1998). The analysis of the electron-impact ionization rates from various sources performed by Avrett and Loeser (2008) revealed a significant scatter, which allows us to calculate these rates using the Seaton (1962) approximate formula with the same uncertainty. The charge exchange with hydrogen was taken into account for neutral oxygen (Arnaud and Rothenflug 1985).

Atomic Data for LTE Elements

The opacity in numerous lines of atoms and their ions is taken into account in the LTE approximation for C–Zn with their solar abundances.⁴ To reduce the computational time, we ignored the lines of atoms and ions whose concentration was less than 10^{-10} of the total concentration of all atoms and ions.

The level energies and statistical weights needed to solve the Saha equations were taken from the NIST database. Model atoms with close energy levels combined into a single one are used to simplify the calculations. However, the number of levels is taken to be large enough for the ionization degree of ions for simplified model atoms to differ by $\lesssim 1\%$ from the corresponding ionization degrees in the case of calculations with all the levels given in NIST.

All of the parameters needed to calculate the lines are read from the special files that are used by the ATLAS12 code (Castelli 2005) to take into account the blanketing effect and that contain the data approximately for 42 million lines.

The photoionization cross sections from the ground and excited states were taken from TOPbase for N I—V, Ne I—VI, Mg I—VI, Al I—VII, Si I—VI, S I—VII, and Ar I—VIII. The photoionization cross sections for C I—IV, O I—VI in the LTE calculations are the same as those in the non-LTE calculations.

SENSITIVITY OF THE RESULTS TO UNCERTAINTIES IN THE ATOMIC DATA AND TO THE ANGULAR DISTRIBUTION OF EXTERNAL RADIATION

Using insufficiently accurate atomic data in the non-LTE modeling can be a source of systematic errors. The atomic data associated with radiative processes for the elements under consideration may be

⁴ The elements C and O were calculated in both LTE and non-LTE, depending on the task.

Table 1. C I—IV energy levels

i	E, cm^{-1}	i	E , cm $^{-1}$	i	E , cm $^{-1}$	i	E, cm^{-1}	i	E, cm ⁻¹
CI		10(20)	77679.8	10	150461.6	4	137425.7	16	311721.5
1	0.0				150466.7		137454.4	17	317794.3
	16.40		80834.6	11	157234.1		137502.0		317796.5
	43.40	CII		12	162517.9	5	145876.1		317801.3
2	10192.6	1	0.0		162524.6	6	182519.9	18	319720.4
3	21648.0		63.42	13	166967.1	7	238213.0	19	321411.3
4	33735.2	2	43003.3		166990.7	8	247170.3		321426.7
5	60333.4		43025.3		167035.7	9	258931.3		321450.1
	60352.6		43053.6	14	168123.7	10	259705.6	20	322003.7
	60393.1	3	74930.1		168124.5		259711.2		322009.6
6	61981.8		74932.6	15	168729.5		259724.3		322018.0
7	64086.9	4	96493.7		168748.3	11	270010.8	CIV	
	64089.9	5	110624.2	16	168978.3		270011.9	1	0.0
	64091.0		110665.6		168978.3		270014.7	2	64484.0
8(10)	68856.3	6	116537.7		C III	12	276482.9	64591.7	
		7	131724.4	1	0.0	13	308216.6	3	302849.0
	73975.9		131735.5	2	52367.06		308248.9	4	320050.1
9	75254.0	8	142027.1		52390.75		308317.3		320081.7
	75255.3	9	145549.3		52447.11	14	309457.2	5	324879.8
	75256.1		145550.7	3	102352.0	15	310006.3		324890.3

i is the ordinal level number, E is the energy of the levels combined into level i. The number in parentheses is the number of combined levels.

considered as quite reliable, while very approximate expressions were used in some cases when the coefficients defining collisional transitions were calculated. Therefore, it is necessary to find out the scale of errors that can be introduced into the model or spectrum of the hot spot due to poor-quality atomic data.

Since only non-LTE models depend on the uncertainty in the collisional transition rates, let us first consider the differences between non-LTE and LTE models, which will give an idea of the scale and pattern of the changes when abandoning LTE. These differences are illustrated for four models in Fig. 2. It

can be seen from this figure that the upper layers of the hot spot cool down, while the inner ones heat up when passing to non-LTE. Despite the fact that the differences in the dependence $T(\tau_{\rm Ross})$ between LTE and non-LTE models are $\lesssim 20\%$, the spectra differ not only qualitatively but also quantitatively.

Comparison shows that non-LTE effects manifest themselves least in hydrogen lines: the central intensity in non-LTE decreases by several tens of percent for models with high $F_{\rm acc}$ and approximately by a factor of 2 for models with low $F_{\rm acc}$. The changes also

202 DODIN

Table 2. O I-IV energy levels

i	E , cm $^{-1}$	i	E , cm $^{-1}$	i	E, cm ⁻¹	i	E, cm ⁻¹	i	E , cm $^{-1}$
OI		O II		O III				O IV	
1	0.0	1	0.0	1	0.0	11	273081.3	1	0.0
	158.265	2	26810.55		113.178	12	283759.7		385.9
	226.977		26830.57		306.174		283977.4	2	71439.8
2	15867.9	3	40468.01	2	20273.27		284071.9		71570.1
3	33792.6		40470.00	3	43185.74	13	290958.3		71755.5
4	73768.2	4	119837.2	4	60324.79	14	293866.5	3	126936.3
5	76795.0		120000.4	5	120025.2		294002.9		126950.2
6	86625.8		120082.9		120053.4		294223.1	4	164366.4
	86627.8	5	165988.5		120058.2	15	324464.9	5	180480.8
	86631.5		165996.5	6	142381.0		324660.8		180724.2
7	88631.2	6	185235.3		142381.8		324839.0	6	231537.5
	88630.6		185340.6		142393.5	16	324735.7	7	255155.9
	88631.3		185499.1	7	187054.0	17	327229.3		255184.9
8	95476.7	7	188888.5	8	197087.7		327278.3	8	289015.4
9	96225.1		189068.5	9	210461.8		327352.2		289023.5
10(8)	97420.6	8	195710.5	10	267258.7	18	329469.8	9	357614.3
		9	203942.3		267377.1		329583.9	10	390161.2
	97488.5	10(6)	206730.8		267634.0		329645.1		390248.0
						19	331821.4	11	419533.9
			206972.7						419550.6

i is the ordinal level number, E is the energy of the levels combined into level i. The number in parentheses is the number of combined levels.

concern the overall shape of the profiles: for example, the ${\rm H}\alpha$ line profile becomes slightly broader and begins to show evidence of an absorption feature at the line center when passing to non-LTE (see Fig. 4). The differences in the spectra for LTE and non-LTE models decrease with increasing line number in the Balmer series.

The fundamental changes in the spectra when passing from LTE to non-LTE happen to the He I lines and especially the He II ones, which are not

formed in LTE under the hot-spot conditions. Such qualitative changes of the spectra are associated with the presence of ionizing external radiation in the atmosphere.

Our modeling shows that the incident radiation with $\lambda < 912$ Å is absorbed mainly by H, He I, and He II atoms, and only at wavelengths 230–400 Å can the absorption by other elements, primarily the C III ion, be important. Therefore, we calculated the

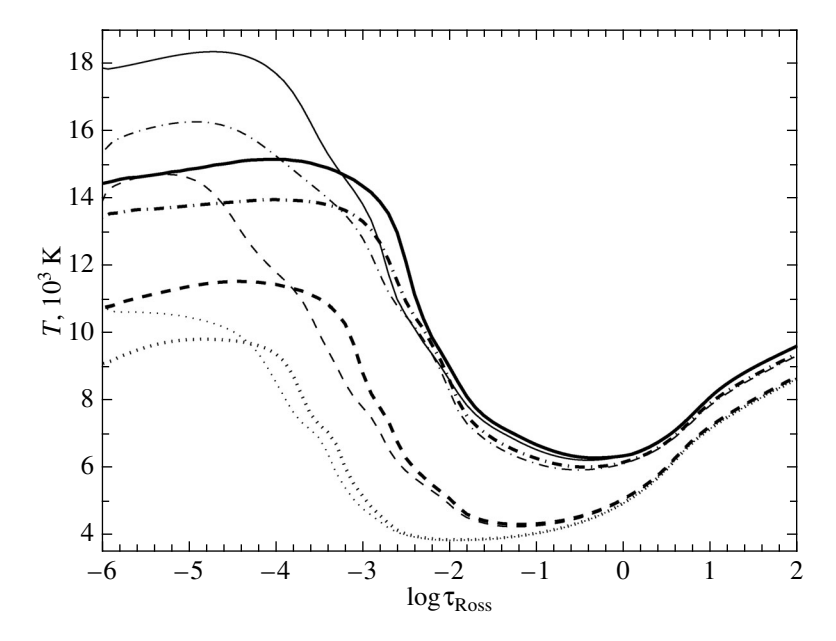


Fig. 2. Comparison of the temperature distributions in the hot spot for the LTE (thin curves) and non-LTE (thick curves) models at various parameters: $V_0 = 250 \text{ km s}^{-1}$, $\log N_0 = 11.5$ (dotted line); $V_0 = 250 \text{ km s}^{-1}$, $\log N_0 = 13$ (dash-dotted line); $V_0 = 400 \text{ km s}^{-1}$, $\log N_0 = 12.5$ (solid line). The temperature of the star is $T_{\rm eff} = 4500 \text{ K}$ and $\log g = 4.0$.

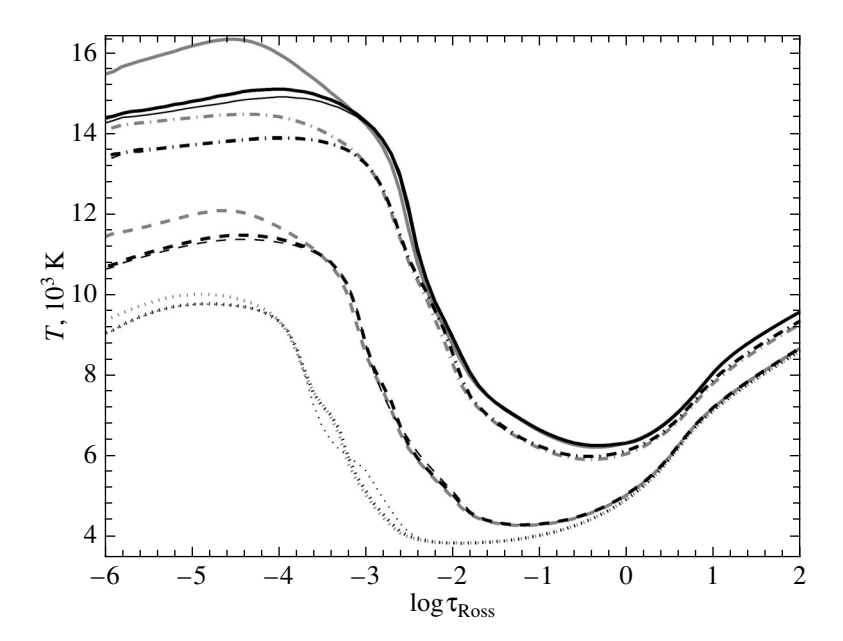
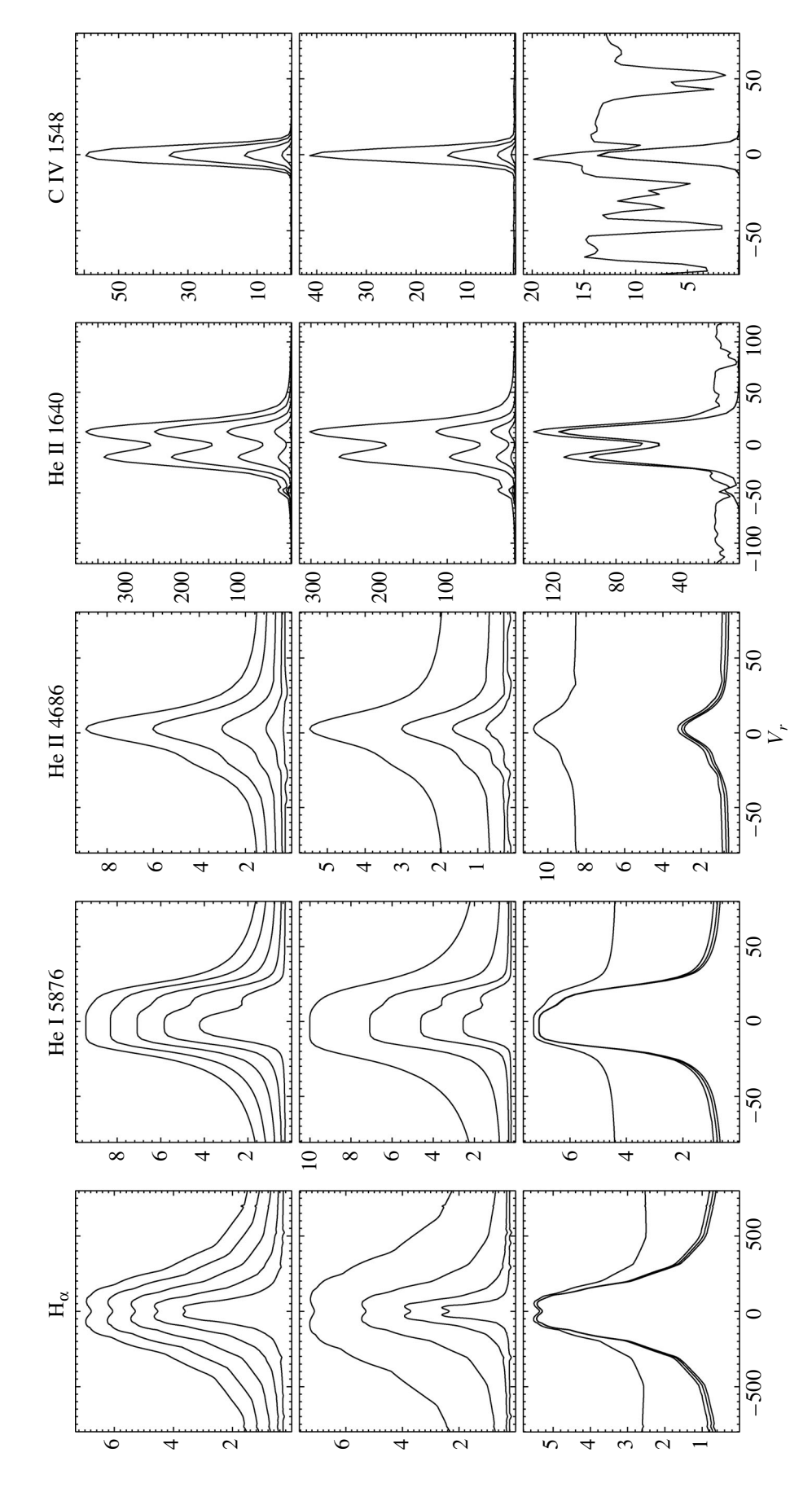


Fig. 3. Temperature distribution in the hot spot in the models that take into account the departures from LTE only for H and He (thick curves) and for H, He, C, and O (thin curves). The gray curves indicate the models with allowance made for the departures from LTE for H and He calculated with the angular distribution of external radiation $I_e(\mu) \propto \mu^{-1}$. The model parameters and the designations of the lines are the same as those in Fig. 2.

models by taking into account the departures from LTE for C I—V. However, no significant influence of non-LTE effects on the model or spectrum of hydrogen and helium was found. Since abandoning LTE for O I—V produced approximately the same effect, adding the next most important elements to the non-

LTE treatment when calculating the model seems like an unjustified complication against a background of the remaining uncertainties. Allowance for higher ionization stages of carbon and oxygen would also be redundant, because the ions with charge +4 already have a negligible concentration, while the dominant



velocity in km s⁻¹ is along the horizontal axis. The upper row: $\log N_0 = 12.5$, $T_{\rm eff} = 4500$ K, $V_0 = 200$, 250, 300, 350, 400 km s⁻¹. The middle row: $V_0 = 300$ km s⁻¹, $\log N_0 = 12.5$, $T_{\rm eff} = 4000$, 4500, 5000, 10000 K. On all panels, the flux rises as the Fig. 4. Changes in the line profiles when varying different parameters. The Eddington flux H_{λ} in units of 10^6 erg s⁻¹ cm⁻² Å⁻¹ sr⁻¹ is along the vertical axis; the radial parameter being varied increases.

ionization stages are C I—III and O I—III, depending on the depth. The temperature distribution in the models with allowance made for the departures from LTE for H, He, C, and O is shown in Fig. 3.

Let us now consider the influence of approximately specified atomic data on the hot-spot spectrum. Using the electron-impact ionization rates for the hydrogen atom calculated using the Johnson (1972) formula and the more approximate Seaton (1962) formula leads to hot-spot spectra that differ in the Balmer and Paschen lines by ~0.1%. Similar calculations for the He I—He II atoms lead to differences of about 0.5% in the optical He I lines and less than 0.1% in He II. Thus, it can be concluded that uncertainties in the electron-impact ionization rates for H, He I, and He II do not affect the structure and spectrum of the hot spot.

An approximate formula from Mihalas (1972) is used for the electron-impact excitation rates from He II levels $n \geq 3$; however, the data for calculating the rate coefficient for the transition from n=3 to n=4 are also given in the book by Sobel'man et al. (2002). Comparison of the results shows that the 4686 Å line calculated with Sobel'man's data strengthens approximately by a factor of 2, while the 1640 Å line weakens by 30%. Such deviations should be kept in mind when comparing calculations with observations.

The accretion-shock spectrum was calculated by Lamzin (1998) only for the flux; however, the angular distribution of external radiation $I_e(\mu)$ should be specified to calculate the models. This introduces an additional uncertainty when constructing the spot model. The true angular distribution of incident radiation must depend on the accretion-column geometry and can be different at different wavelengths; from general considerations, it must be confined between the isotropic distribution $I_e(\mu)=\mathrm{const}$ for $\mu<0$ and $I_e(\mu) \propto \mu^{-1}$ for $\mu < 0$ (in both cases, $I_e(\mu) = 0$ for $\mu > 0$ by the definition of $I_e(\mu)$). This question has already been discussed by Dodin and Lamzin (2012). However, it should be reconsidered in the non-LTE case, because the increase in the mean intensity in the upper layers when passing from the isotropic law to $I_e(\mu) \propto \mu^{-1}$ will lead to a change (enhancement) of the non-LTE effects. Our calculations showed that, as in the LTE model of Dodin and Lamzin (2012), passing from $I_e(\mu) = \text{const to } I_e(\mu) \propto \mu^{-1}$ causes the upper layers to be heated by $\Delta T \sim 100$ K for models with low $F_{\rm acc}$ and by $\Delta T \sim 1000$ K for high $F_{\rm acc}$ (see Fig. 3). At the same time, the deeper layers cool down. The law $I_e(\mu) \propto \mu^{-1}$, in comparison with $I_e(\mu) = \text{const}$, leads to a strengthening of the hydrogen and helium lines by up to 20% and a weakening of the continuum emission by a few percent. The

greatest strengthening is observed for $H\alpha$, but the differences decrease with increasing line number in the series.

DEPENDENCE OF THE SPECTRUM SHAPE ON ACCRETION PARAMETERS

Having estimated the accuracy of the calculated model spectra in the previous section, let us consider the dependence of the spectrum for the hot spot on the basic parameters that must define its structure. Figure 4 presents the profiles of some important lines at typical accretion parameters (Lamzin 1998) $\log N_0 = 11.5, 12, 12.5, 13, V_0 = 200, 250, 300, 350, 400 \ \mathrm{km \ s^{-1}}$ and for a set of stellar effective temperatures $T_{\mathrm{eff}} = 4000, 4500, 5000, 10\,000 \ \mathrm{K}$. In view of the limited computational power, only these parameters were varied, while the remaining ones were fixed: the chemical composition was solar, the surface gravity was $\log g = 4.0$, and the microturbulence was $V_{\mathrm{mic}} = 2.0 \ \mathrm{km \ s^{-1}}$.

The changes in the ${\rm H}\alpha$ line flux are shown in the first column of Fig. 4. It can be seen that the typical width of the hydrogen lines forming in the hot spot is $\gtrsim 100~{\rm km~s^{-1}}$. Consequently, such lines in the observed spectrum will be interpreted as broad emission components whose formation is usually associated with the circumstellar gas rather than with the hot spot (see the Introduction). The hydrogen line width depends strongly on the accretion parameters, increasing with V_0 or N_0 . It may seem that the profile must be defined by a combination of these quantities, for example, only by the ram pressure $P \propto N_0 V_0^2$ or only by the external radiation flux $F_{\rm acc} \propto N_0 V_0^3$, but our checking shows that this is not the case.

As would be expected, the hot spot radiates in narrow He I-He II lines that can be associated with the narrow emission components in the observed spectra of T Tauri stars. In comparison with our previous paper (Dodin et al. 2013), a self-consistent solution of the non-LTE problem led to a strengthening of the He I lines, which now come into explicit conflict with the observations (see the next section). Note that the He I line centroid is redshifted with increasing N_0 or V_0 . This is because the line consists of several fine-structure components that alternately reach saturation, and, consequently, the position of the center of such a composite line depends on its optical depth. In Fig. 4, the wavelength of all fine-structure components averaged over qf is taken as the central wavelength, which corresponds to the optically thin

When calculating the line profiles in Fig. 4, we took into account only the hot-spot emission and disregarded the emission/absorption in the pre-shock and post-shock regions.

The pre-shock region manifests itself in the spectrum in the form of broad components shifted in velocity by $V_0\cos\alpha$, where α is the angle between the line of sight and the streamline of the infalling gas. The pre-shock gas can manifest itself not only in lines but also in continuum, especially at wavelengths shorter than the Balmer jump, where its contribution to the continuum, according to the calculations with the Cloudy code, is comparable to the contribution from the hot spot. Therefore, the calculated hot-spot spectrum cannot be compared with the observations without allowance for the absorption and emission in the infalling gas, especially in the ultraviolet.

The gas in the post-shock region produces lines with a small redshift that can contribute to the narrow component from the red side of the profile. Because of its high ionization, this region does not radiate in HI and HeI lines. However, it can contribute noticeably in He II lines at a free-fall velocity V_0 < 300 km s^{-1} , when these lines are barely formed in the hot spot. The contribution of the post-shock region must increase when passing to the lines of hotter ions. Our non-LTE calculations for CI-IV show that the CIV 1550 doublet lines forming in the hot spot have a very low intensity compared to the He II 1640 line (see Fig. 4), while the observed fluxes in the lines are approximately equal (see the spectra of stars with a distinct narrow component (BP Tau, DS Tau, DN Tau, CY Tau, EG Tau, TWA7, V396 Aur, V397 Aur) in Ardila et al. (2013)). Hence it can be concluded that the narrow component of the C IV 1550 Å doublet lines is formed not in the hot spot but in the post-shock region, as was assumed in Lamzin (2003). Two remarks should be made here. First, greatly simplified atomic models were used to calculate the emission in the C IV doublet lines. Our test calculations show that an increase in the completeness of atomic models for CIII-IV leads to a further weakening of the doublet lines, but the quantitative aspect of the question requires a more detailed consideration. Second, the uncertainty introduced into the UV spectrum by the pre-shock region does not affect this conclusion, because we consider the ratio of narrow line components that are close in wavelengths and, consequently, are distorted identically.

The structure of the outer hot-spot region, where the strong emission lines are formed, is determined mainly by the external radiation and depends weakly on the effective temperature of the accreting star. For this reason, the fluxes in the characteristic hydrogen and helium emission lines are virtually independent of $T_{\rm eff}$ (see the lower row in Fig. 4). This means that at fixed accretion rate and parameters N_0 and V_0 , the contribution of the hot spot to the total spectrum will decrease with increasing temperature and radius of

the star. For example, for a star with a temperature of $10\,000$ K and a radius of $3R_{\odot}$ at an accretion rate of $10^{-7}~M_{\odot}~\rm yr^{-1}$, the typical equivalent widths of the He I 5876 and He II 4686 lines are $\lesssim 0.05$ Å, while these quantities are approximately a factor of 30 larger for a star with a temperature of ~ 4500 K and a radius of $1.5~R_{\odot}$.

COMPARISON OF THE MODEL SPECTRA WITH OBSERVATIONS

As has been noted in the Introduction, using the LTE hot-spot structure, Dodin et al. (2013) calculated the non-LTE helium spectrum, but they failed to simultaneously reproduce the intensity of the He I and He II lines observed in the spectra of CTTS. The authors suggested that this difficulty could be overcome if the hot-spot structure was calculated by abandoning the LTE approximation, which has been done in this paper.

It turned out that the helium problem could actually be solved, but new difficulties arise in this case. These will be demonstrated using the star TW Hya as an example, whose spectrum was taken on May 3, 2011, with the X-shooter spectrograph on one of the VLT telescopes. The spectrum was retrieved from the ESO archive and reduced with the X-Shooter pipeline (version 2.5.0) following the user manual.⁵

To demonstrate the essence of the arising problems more clearly, let us make two simplifying assumptions. First, we will assume that the accretion zone consists of a large number of hot spots that are distributed uniformly over the visible hemisphere of the star and are characterized by the same values of N_0 and V_0 . This allows us not to introduce any additional parameters describing the location and shape of the accretion zone and to use the emergent flux H_{λ} instead of the intensity $I_{\lambda}(\mu)$. By the way, Calvet and Gullbring (1998) used precisely this approximation. Second, we will assume that the pre-shock gas is transparent to the hot-spot radiation. Therefore, we can simply add its intrinsic radiation H_{pre} to the hotspot radiation $H_{\rm hs}$ and, just as in Calvet and Gullbring (1998), represent the observed flux from the star+spot system as

$$F = C \left[f(H_{hs} + H_{pre}) + (1 - f)H_* \right],$$

where C is the normalization constant, f is the ratio of the total area of the accretion spots to the area of the visible hemisphere (filling factor), and H_* is the flux from the star calculated with the ATLAS9 and SYNTHE codes (Castelli and Kurucz 2004; Sbordone et al. 2004). Our estimates made with the

⁵ ftp://ftp.eso.org/pub/dfs/pipelines/xshooter/
xshoo-pipeline-manual-12.3.pdf

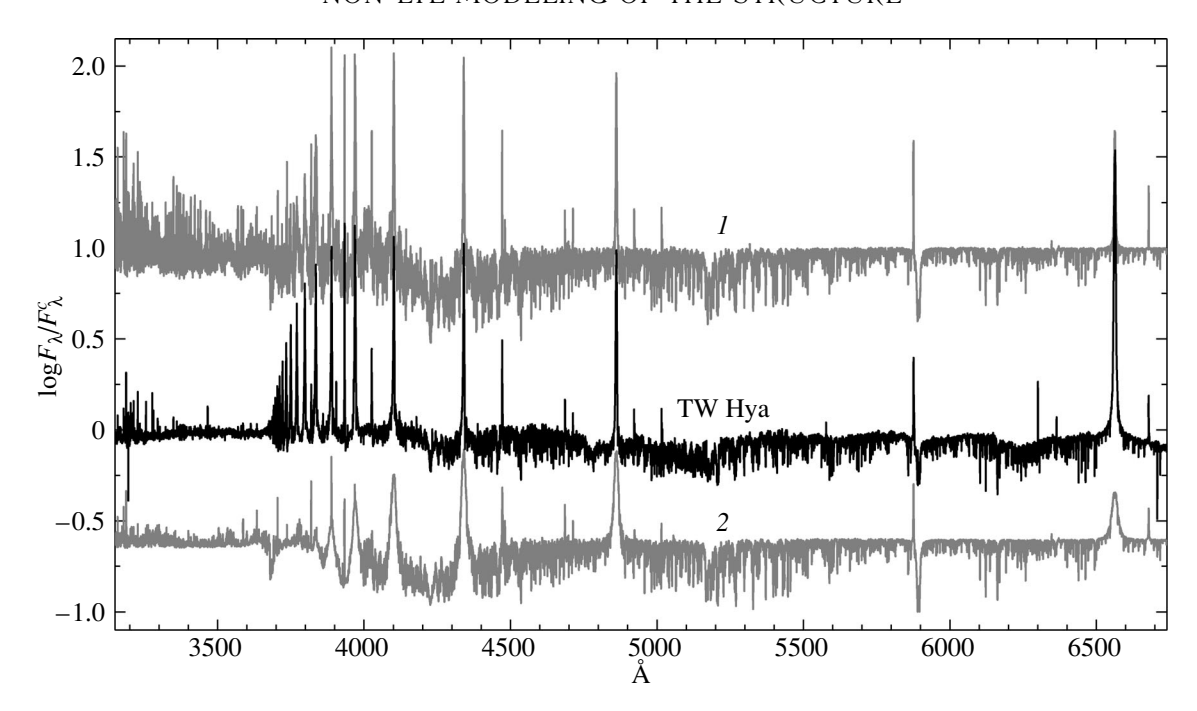


Fig. 5. The black curve at the center indicates the logarithm of the observed spectrum normalized to the continuum for TW Hya. The gray curves indicate the theoretical spectra shifted along the y axis by some values for the convenience of comparison. The spectrum (I) was calculated for the following parameters: $T_{\rm eff}=4000~{\rm K}$, $\log g=4.0$, microturbulence $V_{\rm mic}=2~{\rm km~s^{-1}}$, $V_0=300~{\rm km~s^{-1}}$, $N_0=10^{12}~{\rm cm^{-3}}$, and f=0.11. The spectrum (2) was calculated for the same parameters but at $V_0=350~{\rm km~s^{-1}}$, $N_0=10^{13}~{\rm cm^{-3}}$, and f=0.016. The theoretical spectrum was convolved with a Gaussian profile in such a way that the absorption line widths roughly corresponded to the observed ones.

Cloudy code show that the infalling gas at the parameters under consideration is indeed transparent in continuum, at least for $\lambda > 3650$ Å.

There is no reliable technique for determining the fundamental parameters of T Tauri stars that would adequately take into account the accretion and spottedness of these stars. This is probably responsible for the significant scatter of effective temperature estimates for TW Hya provided by various authors: $T_{\rm eff}=3400-4200$ K (Vacca and Sandell 2011; Yang et al. 2005). Therefore, for our comparison with the observations, we used the models of a star with $T_{\rm eff}=3500-4500$ K and $\log g=3.5-4.5$, but the character of the fundamental contradictions with the observations does not depend on specific parameters and will be illustrated for $T_{\rm eff}=4000$ K and $\log g=4.0$.

Comparison of the theoretical and observed hydrogen line widths leads to the conclusion about a low density, $N_0 \sim 10^{12}$ cm⁻³. At such a density, the H β – H δ lines, along with the He I and He II lines, can be reproduced (see the spectrum (1) in Figs. 5 and 6). In this case, however, the theoretical depth of the absorption lines turns out to be larger than the observed one, especially in the blue region of the spectrum (see Fig. 6). The possibility that the discrepancy in absorption line depths is due to our simplifying assumptions must not be ruled out. However, irrespective of

this, the hydrogen emission lines up to H_{20} are visible in the spectrum of TW Hya, while the lines higher than H_{10} are indistinguishable in the hot-spot spectrum at any N_0 and V_0 . Furthermore, the observed equivalent width of the $H\alpha$ line in TW Hya turns out to be considerably larger than the theoretical one. Hence it can be concluded that the hydrogen lines are formed not only in the hot spot but also outside it, in a region with a lower density. Thus, the theoretical reproduction of the observed hydrogen spectrum is meaningless without allowance for the circumstellargas radiation. The hot-spot parameters can be found without resorting to the hydrogen lines. In this case, a relatively high density of the infalling gas, $N_0 \sim$ 10^{13} cm⁻³, is required to reconcile the depths of the star's absorption lines and He I-He II emission lines with the observations (see the spectrum (2) in Figs. 5 and 6), just as in Dodin et al. (2013). However, the hydrogen lines at such densities become so broad that their wings extend beyond the observed profile.

The hydrogen line spectrum originating in the hot spot has not yet been calculated by anybody. Therefore, the conclusion that the hydrogen spectrum and the degree of veiling in the spectra of CTTS cannot be simultaneously reproduced with a single set of accretion parameters N_0 and V_0 is new and of great interest from the standpoint of accretion shock diagnostics.

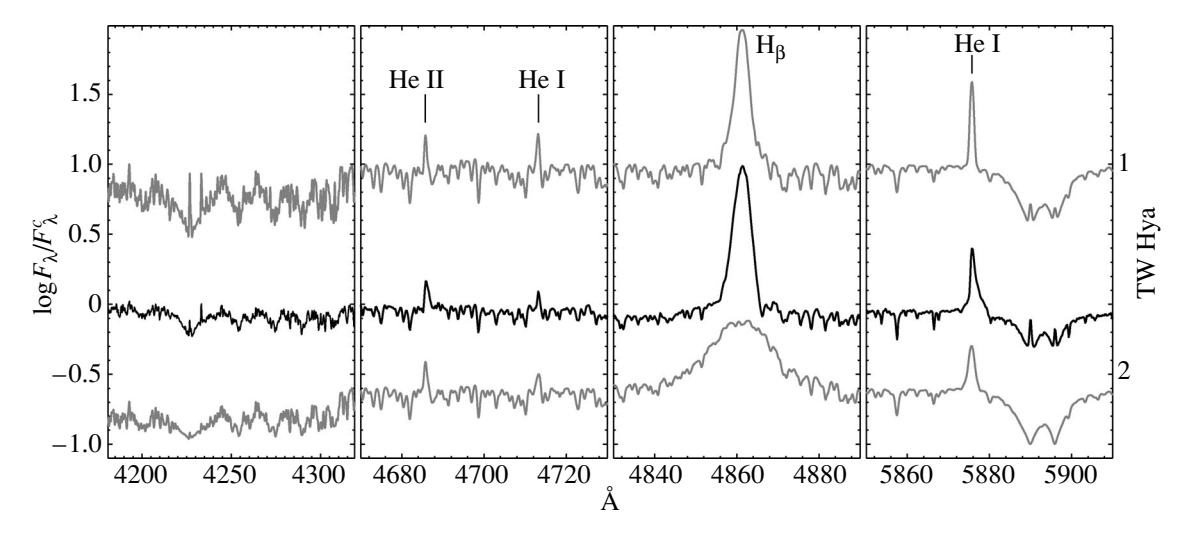


Fig. 6. Magnified regions of the spectra shown in Fig. 5. It can be seen on the first panel that the absorption lines in the spectrum (1) are much stronger than those in the observed spectrum.

It seems quite natural from general considerations that the accretion is inhomogeneous in a real situation. Moreover, Dodin et al. (2013) and Ingleby et al. (2013) argue that the observed spectra of CTTS are a sum of the contributions from regions with various N_0 and V_0 . Using the hydrogen spectrum for diagnostics forces us to look at the problem of spot inhomogeneity afresh: since the veiling continuum is definitely formed in the hot spot and since high densities, $\log N_0 > 12.0$, are required to explain the observed degree of veiling, there is a need to somehow weaken the hydrogen line emission from this (inhomogeneous) hot-spot region.

CONCLUSIONS

In this paper, we presented the models of hot accretion spots on the surface of young stars calculated by taking into account the non-LTE effects for hydrogen and helium. At nearly solar elemental abundances, C and O are the next most important absorbers of the incident ionizing radiation after H and He, and their inclusion did not lead to significant changes in the model. Hence it can be concluded that the influence of non-LTE effects on the hot-spot structure related to the differences in the absorption of the incident radiation in the LTE and non-LTE cases was taken into account fairly completely. Allowance for the non-LTE effects in the remaining elements that determine the opacity at optical wavelengths can in principle lead to changes in the model atmosphere, but these changes will probably be approximately the same as those for main-sequence stars with effective temperatures of the order of the effective temperature for the hot spot (<10000 K), i.e., negligibly small (Hauschildt et al. 1999).

We obtained the Eddington flux H_{λ} as a byproduct of calculating the model atmosphere. Its analysis allowed us to reach several new conclusions: the broad hydrogen line wings can be formed in the hot spot; the lines of "hot" ions, such as C IV, are barely formed in the models under consideration.

We failed to consistently describe the observed spectrum of the star TW Hya using a single set of N_0 and V_0 on the precalculated grid of spectra in the ranges of parameters $\log N_0 = 11.5 - 13$ and $V_0 =$ $200-400 \text{ km s}^{-1}$. This is because to obtain the required ratio between the helium lines and continuum, we must use the models with $N_0 \sim 10^{13}~{\rm cm}^{-3}$, but in this case we obtain hydrogen line profiles that are considerably broader than the observed ones. This problem can possibly be solved by assuming the simultaneous existence of regions with $\log N_0 < 13$ and regions with a higher density N_0 , at which the infalling gas becomes optically thick in continuum, in the accretion zone. In this case, an observer will see no radiation from the heated atmosphere, because the shock photosphere will be in the freely falling gas, i.e., ahead of the accretion shock front.

The spectrum of such a gas must resemble the spectrum of a star with $T_{\rm eff} \sim (F_{\rm acc}/\sigma)^{0.25} \gtrsim 10\,000$ K: there must be evidence of hydrogen and helium lines that are in absorption and redshifted in the spectrum. Such features are observed in the spectrum of some CTTS; in particular, an absorption feature in the hydrogen lines with a maximum depth at a radial velocity of about $+300~{\rm km~s^{-1}}$ can be revealed in the presented spectrum of TW Hya. To test the validity of this explanation, the structure and spectrum of the pre-shock gas should be modeled in more detail (than was done in this paper) for an extended range of N_0 . Such modeling is a topical problem, because the lines

forming in the infalling gas can be informative for accretion diagnostics and already begin to be used for these purposes (Petrov et al. 2014).

The calculated grid of hot-spot models and spectra with allowance made for the departures from LTE for hydrogen and helium is accessible at the following address: lnfm1.sai.msu.ru/~davnv/hotspot.

ACKNOWLEDGMENTS

I wish to thank V.P. Grinin, S.A. Lamzin, and L.I. Mashonkina for the useful discussions and the anonymous referees for the remarks that allowed the text of the paper to be improved. This work was supported by the "Dynasty" Foundation and the Program for Support of Leading Scientific Schools (NSh-261.2014.2). Based on observations made with ESO Telescopes at the La Silla Paranal Observatory under Programme ID 085.C-0764(A).

REFERENCES

- K. M. Aggarwal and F. P. Keenan, Astrophys. J. Suppl. Ser. 123, 311 (1999).
- K. M. Aggarwal and F. P. Keenan, Astron. Astrophys. 486, 1053 (2008).
- 3. C. W. Allen, *Astrophysical Quantities*, 3rd ed. (Athlone Press, London, 1973).
- D. R. Ardila, G. J. Herczeg, S. G. Gregory, L. Ingleby, K. France, A. Brown, S. Edwards, C. Johns-Krull, et al., Astrophys. J. Suppl. Ser. 207, 1 (2013).
- 5. M. Arnaud and R. Rothenflug, Astron. Astrophys. Suppl. Ser. **60**, 425 (1985).
- L. H. Auer and D. Mihalas, Astrophys. J. Suppl. Ser. 24, 193 (1972).
- 7. E. H. Avrett and R. Loeser, Astrophys. J. Suppl. Ser. **175**, 229 (2008).
- 8. P. S. Barclem, Astron. Astrophys. 462, 781 (2007).
- 9. C. C. Batalha, N. M. Stout-Batalha, G. Basri, and M. A. O. Nerra, Astrophys. J. Suppl. Ser. 103, 211 (1996).
- V. B. Berestetskii, E. M. Lifshitz, and L. P. Pitaevskii, Course of Theoretical Physics, Vol. 4: Quantum Electrodynamics (Nauka, Moscow, 1989; Pergamon, Oxford, 1982).
- 11. A. K. Bhatia and S. O. Kastner, Astrophys. J. Suppl. Ser. **96**, 325 (1995).
- 12. I. Bray, A. Burgess, D. V. Fursa, and J. A. Tully, Astron. Astrophys. Suppl. Ser. **146**, 481 (2000).
- 13. K. Butler and J. Giddings, in *Newsletter of Analysis of Astronomical Spectra* (Univ. London, London, 1985), No. 9.
- N. Calvet and E. Gullbring, Astrophys. J. **509**, 802 (1998).
- F. Castelli and R. L. Kurucz, astro-ph/0405087 (2004).
- 16. F. Castelli, Mem. Soc. Astron. It. Suppl. 8, 25 (2005).
- R. E. H. Clark, J. Abdallah, Jr., and J. B. Mann, Astrophys. J. 381, 597 (1991).

- 18. K. P. Dere, E. Landi, and H. E. Mason, Astron. Astrophys. Suppl. Ser. **125**, 149 (1997).
- M. S. Dimitrijevic and S. Sahal-Brechot, J. Quant. Spectrosc. Radiat. Transfer 31, 301 (1984).
- 20. A. V. Dodin, S. A. Lamzin, and G. A. Chuntonov, Astron. Lett. 38, 167 (2012).
- A. V. Dodin and S. A. Lamzin, Astron. Lett. 38, 649 (2012).
- 22. A. V. Dodin, S. A. Lamzin, and T. M. Sitnova, Astron. Lett. **39**, 315 (2013).
- 23. S. Dreizler, ASP Conf. 288, 69 (2003).
- 24. G. J. Ferland, K. T. Korista, D. A. Verner, J. W. Ferguson, J. B. Kingdon, and E. M. Verner, Publ. Astron. Soc. Pacif. 110, 761 (1998).
- 25. C. F. Fischer and G. Tachiev, Atom. Data Nucl. Data Table 87, 1 (2004).
- 26. A. I. Gomez de Castro and B. von Rekowski, Mon. Not. R. Astron. Soc. 411, 849 (2011).
- 27. H. R. Griem, Astrophys. J. 132, 883 (1960).
- 28. D. C. Griffin, N. R. Badnell, and M. S. Pindzola, J. Phys. B: At. Mol. Opt. Phys. **33**, 1013 (2000).
- H. M. Günther and A. C. Wawrzyn, Astron. Astrophys. 526, 117 (2011).
- 30. P. H. Hauschildt, F. Allard, and E. Baron, Astrophys. J. **512**, 377 (1999).
- 31. L. Ingleby, N. Calvet, G. Herczeg, A. Blaty, F. Walter, D. Ardila, R. Alexander, S. Edwards, et al., Astrophys. J. **767**, 112 (2013).
- 32. L. C. Johnson, Astrophys. J. 174, 227 (1972).
- 33. R. Kisielius, P. J. Storey, G. J. Ferland, and F. P. Keenan, Mon. Not. R. Astron. Soc. **397**, 903 (2009).
- 34. A. Königl, Astrophys. J. **370**, L39 (1991).
- 35. F. Kupka, N. Piskunov, T. A. Ryabchikova, H. C. Stempels, and W. W. Weiss, Astron. Astrophys. Suppl. Ser. 138, 119 (1999).
- 36. R. Kurucz, SAO Sp. Rep. **309** (1970).
- 37. S. A. Lamzin, Astron. Rep. 42, 322 (1998).
- 38. S. A. Lamzin, Astron. Rep. 47, 498 (2003).
- 39. E. Landi, G. Del Zanna, P. R. Young, K. P. Dere, H. E. Mason, and M. Landini, Astrophys. J. Suppl. Ser. **162**, 261 (2006).
- 40. B. M. McLaughlin and K. L. Bell, Astrophys. J. Suppl. Ser. **94**, 825 (1994).
- 41. D. Mihalas, NCAR-TN/STR-76 (1972).
- 42. D. Mihalas and M. E. Stone, Astrophys. J. **151**, 293 (1968).
- 43. D. M. Mitnik, D. C. Griffin, C. P. Ballance, and N. R. Badnell, J. Phys. B: At. Mol. Opt. Phys. **36**, 717 (2003).
- 44. A. S. Mitskevich and V. V. Tsymbal, Astron. Astrophys. **260**, 303 (1992).
- 45. S. N. Nahar, Astrophys. J. Suppl. Ser. **101**, 423 (1995).
- 46. S. N. Nahar, Phys. Rev. A 58, 3766 (1998).
- 47. S. N. Nahar, New Astron. **15**, 417 (2010).
- 48. S. N. Nahar and A. K. Pradhan, Phys. Rev. A 44, 2935 (1991).
- 49. S. N. Nahar and A. K. Pradhan, Phys. Rev. A **49**, 1816 (1994).

- 50. S. N. Nahar and A. K. Pradhan, Astrophys. J. Suppl. Ser. **111**, 339 (1997).
- I. C. Percival and D. Richards, Mon. Not. R. Astron. Soc. 183, 329 (1978).
- 52. P. P. Petrov, G. F. Gahm, G. J. Herczeg, H. C. Stempels, and F. M. Walter, Astron. Astrophys. **568**, L10 (2014).
- 53. N. Przybilla, Astron. Astrophys. **443**, 293 (2005).
- 54. N. Przybilla and K. Butler, Astrophys. J. **609**, 1181 (2004).
- 55. H. van Regemorter, Astrophys. J. **136**, 906 (1962).
- 56. R. H. G. Reid, JET-R(94)06 (1994).
- 57. M. M. Romanova, G. V. Ustyugova, A. V. Koldoba, and R. V. E. Lovelace, Astrophys. J. **610**, 920 (2004).
- 58. N. A. Sakhibullin and V. V. Shimanskii, Astron. Rep. **40**, 62 (1996).
- 59. L. Sbordone, P. Bonifacio, F. Castelli, and R. L. Kurucz, Mem. Soc. Astron. It. Suppl. **5**, 93 (2004).
- 60. T. Schöoning and K. Butler, Astron. Astrophys. Suppl. Ser. 78, 51 (1989).

- 61. M. J. Seaton, *Atomic and Molecular Processes* (Academic Press, New York, 1962).
- 62. C. Stehle and R. Hutcheon, Astron. Astrophys. Suppl. Ser. **140**, 93 (1999).
- 63. W. D. Vacca and G. Sandell, Astrophys. J. **732**, 8 (2011).
- 64. I. I. Sobel'man, L. A. Vainshtein, and E. A. Yukov, *Excitation of Atoms and Broadening of Spectral Lines* (Nauka, Moscow, 1979; Springer, New York, 2002).
- 65. N. J. Wilson, K. L. Bell, and C. E. Hudson, Astron. Astrophys. **432**, 731 (2005).
- 66. H. Yang, C. M. Johns-Krull, and J. A. Valenti, Astrophys. J. **635**, 466 (2005).

Translated by V. Astakhov